Leveraging Google Earth Engine platform to characterize and map small seasonal wetlands in the semi-arid environments of South Africa

Siyamthanda Gxokwe *, Timothy Dube, Dominic Mazvimavi

Institute for Water Studies, Department of Earth Science, University of the Western Cape, Private Bag X17, Bellville, 7535 Cape Town, South Africa

HIGHLIGHTS

- There is a great concern that small semi-arid wetlands are not routinely monitored.
- Monitoring of small wetlands using optical data has remained a challenge.
- Google Earth Engine platform was used to study small wetlands in Limpopo.
- Google Earth Engine provides new opportunities to improve wetlands monitoring.
- Findings underscore the relevance of GEE in studying small and seasonal wetlands.

GRAPHICAL ABSTRACT
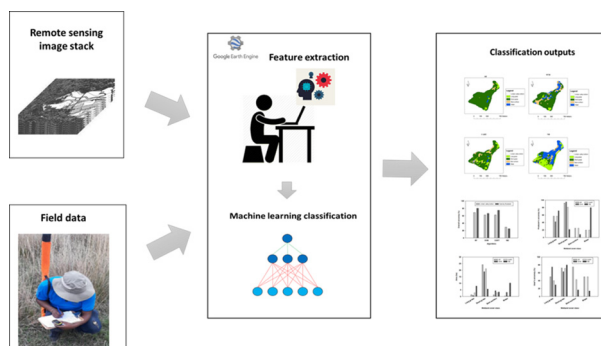
ARTICLE INFO

ABSTRACT

Although significant scientific research strides have been made in mapping the spatial extents and ecohydrological dynamics of wetlands in semi-arid environments, the focus on small wetlands remains a challenge. This is due to the sensing characteristics of remote sensing platforms and lack of robust data processing techniques. Advancements in data analytic tools, such as the introduction of Google Earth Engine (GEE) platform provides unique opportunities for improved assessment of small and scattered wetlands. This study thus assessed the capabilities of GEE cloud-computing platform in characterising small seasonal flooded wetlands, using the new generation Sentinel 2 data from 2016 to 2020. Specifically, the study assessed the spectral separability of different land cover classes for two different wetlands detected, using Sentinel-2 multi-year composite water and vegetation indices and to identify the most suitable GEE machine learning algorithm for accurately detecting and mapping semi-arid seasonal wetlands. This was achieved using the object based Random Forest (RF), Support Vector Machine (SVM), Classification and Regression Tree (CART) and Naïve Bayes (NB) advanced algorithms in GEE. The results demonstrated the capabilities of using the GEE platform to characterize wetlands with acceptable accuracy. All algorithms showed superiority, in mapping the two wetlands except for the NB method, which had lowest overall classification accuracy. These findings underscore the relevance of the GEE platform, Sentinel-2 data and advanced algorithms in characterizing small and seasonal semi-arid wetlands.

© 2021 Elsevier B.V. All rights reserved.

1. Introduction

Wetlands play a critical role in the hydrological cycle and sustaining livelihoods and aquatic life and biodiversity. They occupy transition zones between aquatic and terrestrial environments and share the characteristics of both zones (Gxokwe et al., 2020). Wetlands cover about 4-6% of the global land surface and are ranked amongst the very diverse ecosystems on earth (Mahdianpari et al., 2019). Semi-arid areas are dominated by small seasonally or intermittently flooded wetlands, with the flooded area depending on the balance between precipitation and evapotranspiration (Ruiz, 2008). They often host more invertebrates than permanently inundated systems because of their oxygenated period resulting from the episodic inundation. However their conservation is not prioritised (Chen and Liu, 2015). This is mainly due to their small size and ephemeral nature, which results in them being neglected in monitoring and management programmes, leading to loss of inherent ecosystems goods and services provision (Li et al., 2015).

Globally, the abundance and quality of wetlands in semi-arid environments are reported to be declining due to climate change and variability as well as poor land management practices (Mahdianpari et al., 2019). Gebresllassie et al. (2014) reported a significant wetland loss in the semi-arid Ethiopia due to lack of policies safeguarding these systems, thus resulting in the loss of socio-economic services. In semi-arid parts of China, it has been reported that about 30% of wetlands have been lost over the past 50 years due to anthropogenic activities, with most of them disappearing between 1990 and 2000 (Liu et al., 2017). In South Africa, it is reported that over 50% of wetlands have been eradicated in some catchments due to climate change and anthropogenic activities (Day et al., 2010). Given the significance of ecological services provided by wetlands, it is imperative that these systems are sustainably managed.

The basis for sustainable management of wetlands is hinged on frequent monitoring of their ecohydrological dynamics to derive consistent and comparable information, which is lacking in most semi-arid regions, especially in sub-Saharan Africa (Mahdianpari et al., 2019). The availability of earth observation data offers an opportunity to map and monitor wetlands in a spatially explicit manner in different climatic regions, lacking monitoring systems (Gxokwe et al., 2020). The challenge however is that these data come in a range of spatial, spectral and temporal resolutions which presents difficulties mapping semi-arid wetlands using coarse to medium resolution data such as Moderate Resolution Imaging Spectroradiometer (MODIS).

Wetlands in the semi-arid regions are mostly heterogeneous, with no definitive boundaries, and are spectrally similar to the surrounding landscapes. This results in difficulties when separating these systems from the surrounding landscapes using the coarse to medium spatial resolution data (Mahdianpari et al., 2020). High resolution data such as Wordview-2 and Satellite Pour I'Obeservation de la Terre (SPOT 6-7) are commercial and require complex processing algorithms and are therefore not feasible for monitoring spatial characteristics of semi-arid wetland over large areas and overtime (Gxokwe et al., 2020).

Advancements in data analytic tools and platforms and the development of cloud computing platforms such as Microsoft Azure (MA), Amazon web services (AWS) and Google Earth Engine (GEE) provide wetlands monitoring and assessment across various scales. The AWS was launched in 2006 and contains several remote sensing data ranging from Sentinel-1, Sentinel-2, Landsat 8, and National Oceanographic and Atmospheric Administration (NOAA), Advanced High-Resolution Rapid Refresh Model (AHRRRM) (Tamiminia et al., 2020). Although AWS provides unique benefits through access to a large suite of machine learning algorithms and artificial intelligence, the platform offers pay-as-you go services. Microsoft Azure was launched in 2010 for building, deploying and managing applications and services through Microsoft-managed data centres. The platform consists of advanced machine learning algorithms, Landsat and Sentinel-2 data from 2013 to present for only North America as well as MODIS data from 2000 to present.

The recently introduced GEE platform offers a parallelised processing on Google cloud enabling the processing of a stack of images at once rather than relying on a single date image. The platform has 40 years petabyte scale of pre-processed remotely sensed data, which include Landsat, MODIS, National Oceanographic and Atmospheric Administration Advanced Very High-Resolution Radiometer (NOAA AVHRR), Sentinel 1, 2, 3 and 5-P; and Advanced Land Observing Satellite (ALOS) data as well as advanced machine learning algorithms (Amani et al., 2020). The other data types available on the GEE cloud computing platform include climate and geophysical data, as well as ready to use products such as Normalised Difference Vegetation Index (NDVI) and Enhanced Vegetation index (EVI) (Gorelick et al., 2017).

Although the GEE was launched over a decade ago, its application to remote sensing of wetlands including the small seasonally flooded systems in the semi-arid regions is still limited. A review by Tamiminia et al. (2020) reported 13 wetlands and mangroves studies that utilized the GEE platform between the year 2010 and 2019 in all climatic zones, with most of these studies exploiting Landsat 8 data. The review by Kumar and Mutanga (2018) also reported that of 8% (out of the 300 articles identified) of the studies utilized the GEE platforms for wetlands and hydrological related research globally. The most recent studies by Mahdianpari et al. (2019, 2020) used the GEE to monitor semi-arid wetlands in Canada with reasonable accuracies (70% - 90%), however, the studies focused on large-scale mapping. Due to the strengths of the GEE cloud computing platform, there is therefore a need to fully explore the capabilities of this platform in mapping and determining characteristics of semi-arid wetlands at site specific scales. This is particularly relevant in the sub-Saharan Africa where small wetlands are poorly documented, the application of the GEE on small seasonal wetlands is still lacking, and data on these systems is inconsistent and incomparable due to limited research.

Owing to this background, the overarching goal of this study was to characterize and map two small and seasonally flooded wetlands in the semi-arid Limpopo Transboundary River Basin in South Africa using the GEE cloud-computing platform and the multi-year Sentinel-2 composite data. Specifically, the objectives were to; (1) assess the spectral separability of different wetland cover classes detected, using the GEE and multi-year Sentinel-2 composite derivatives; (2) evaluate the capabilities of GEE cloud-computing platform in producing customized wetland cover maps at reasonable accuracy, using the high-resolution Sentinel-2 data, and (3) identify a suitable GEE machine learning algorithm for accurately detecting and mapping semi-arid seasonal wetlands characteristics, using the multi-year Sentinel 2 composite data. The paper is organised as follows. Section 1 provides a detailed background of the study including scientific knowledge gaps and the objectives of the study. Section 2 shows how the GEE cloud computing platform coupled with the field and remote sensing data were used in achieving the objectives of this paper. The findings of the study are presented in Section 3. Sections 4 and 5 present interpretations, conclusions and recommendations drawn from the study findings.

2. Study area

Two wetlands located in the Limpopo Transboundary River Basin in South Africa (LTRB) were investigated (Fig. 1). The LTRB is shared by four countries namely South Africa, Botswana, Mozambique and Zimbabwe, and covers an area of 412,000 km^2 (Mosase et al., 2019). The basin has a semi-arid climate, with wet summers and dry winters. The Mean Annual Precipitation (MAP) in the LTRB ranges from 300 to 700 mm/year with most of the rainfall occurring during the October to April period (Botai et al., 2020). Temperatures in the LTRB follow a distinct seasonal cycle with the coolest months occurring in winter (June-August), and hottest occurring in late summer (late November- early December). The mean daily temperatures in LTRB can go up to 40 °C

(Sawunyama et al., 2006). The mean annual evaporation varies between 1600 mm/yr and 1700 mm/yr in the south-eastern mountainous region, and from 2600 mm/yr to 3100 mm/yr in the western and central regions (Sawunyama et al., 2006). The two studied seasonal flooded wetlands are the Nylsvley floodplain and Lindani valley bottom in South Africa. The Nylsvley floodplain is Ramsar protected system located at 24°39′17″S and 28°41′28″E near Mookgopong and Modemolle towns in the Limpopo Province of South Africa. The wetland forms a 70 km long floodplain along Mogalakwena River, which is a tributary of the Limpopo River (Dzurume, 2021). The dominant vegetation species occurring in the Nylsvley floodplain include common grass species such as *Oryza longistaminata* (rice grass) and *Phragmites australis* (common reeds), and tree species such as *Acacia tortilis*, *Acacia nilotica* and *Acacia karoo*. The Nylsvley floodplain receives most of the inflows from seasonal rivers such as Olifantsspruit, Groot and Klein Nyl (Dzurume, 2021). Although the floodplain is 70 km long, the study focuses on the 13.69 km² portion within the boundaries of the Nyls Nature Reserve, which was accessible during the study period. The Lindani valley bottom wetland is located between 24°03′01.36″E and 28°41′43.37″S within the boundaries of the Lindani Private Game Reserve at Vaalwater Limpopo Province of South Africa. The wetland covers an area of about 28 ha and mostly receives water from rainfall and groundwater seeps from several springs in the area. The dominant vegetation species include the *Oryza longistaminata* (rice grass), *Phragmites australis* (common reeds), *Scirpoides dioecus* (Kunth) as well as *Cynodon dyctolon* (Bermuda grass).

3. Materials and methods

3.1. Field data

Land cover data were collected in the field during the end of the dry season and beginning of wet season between the 28th of September 2020 and the 1st of October 2020. The data collected included six hundred ground truth points collected on both wetlands with locations determined used a handheld Geographical Positioning System (GPS) with less than 5% error. The points were collected using a stratified random sampling approach. This approach involves the division of a population into smaller subgroups named strata based on certain attributes, and random sampling is implemented on the strata (Ding et al., 1998). Stratified random sampling was selected because of the possibility that each sample is equally likely to occur. During the implementation of stratified random sampling in this study, the wetlands were subdivided into 10 m × 10 m quadrants based on the Sentinel-2-pixel sizes data that was going to be used during the classification process. The quadrants were 12 m apart in order to minimise overlapping samples on the satellite image. In each quadrant a maximum of 20 ground truth points were collected depending on the dominating landcover classes. Moreover, wetland vegetation communities were visually identified on site and grouped as either short grass and long grass species based on structural features (canopy height and cover). The collected data were used in the GEE wetland model training, and validating satellite derived wetland cover classes.
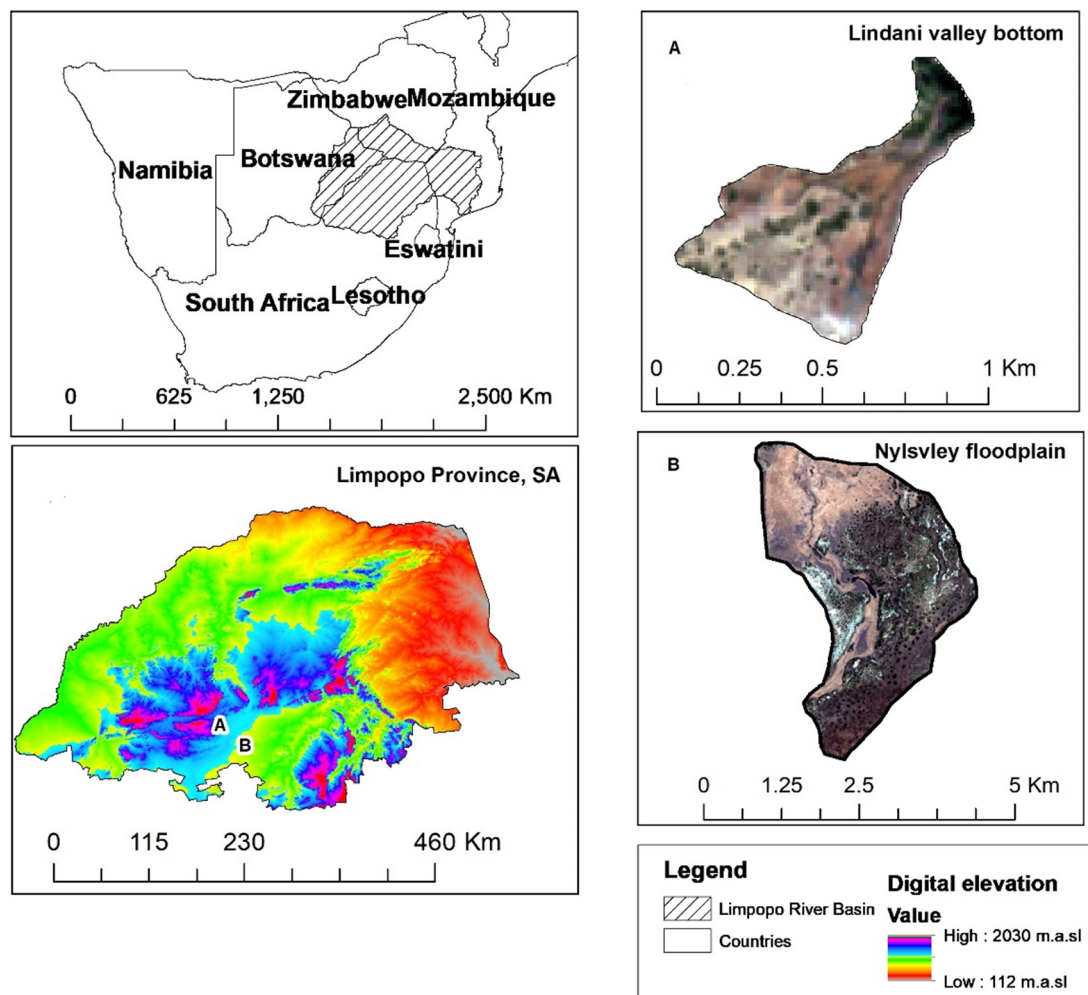

Fig. 1. Location of the studied wetlands, a) Lindani valley bottom b) Nylsvley floodplain within the Limpopo Transboundary River Basin.

3.2. Remote sensing data acquisition and processing

The acquisition and processing of remotely sensed data in this study were executed following the steps shown on Fig. 2. Sentinel-2 MultiSpectral Instrument (MSI), level 2A (COPERNICUS/S2_SR/20151128T002653_20151128T102149_T56MNN) Surface reflectance images were acquired from the GEE database and used in this study. These products are already atmospherically corrected using the Sen2cor and contain twelve UINT16 spectral bands scaled by 10,000 as well as three QA bands where one (QA60) is a bitmask band with cloud mask information. The image stack was filtered to represent the period of 2016-01-01 to 2020-12-31, and the area within the selected wetland boundaries using the codes ee.Filter.Date ( ) and Image.filterBounds ( ). The period was chosen because in 2016, drought was reported in the Limpopo Basin, which caused significant changes in most surface water systems including wetlands in the area. The study aimed to establish whether drought induced changes within the wetlands could be determined. Two hundred ninety-six images were obtained after the
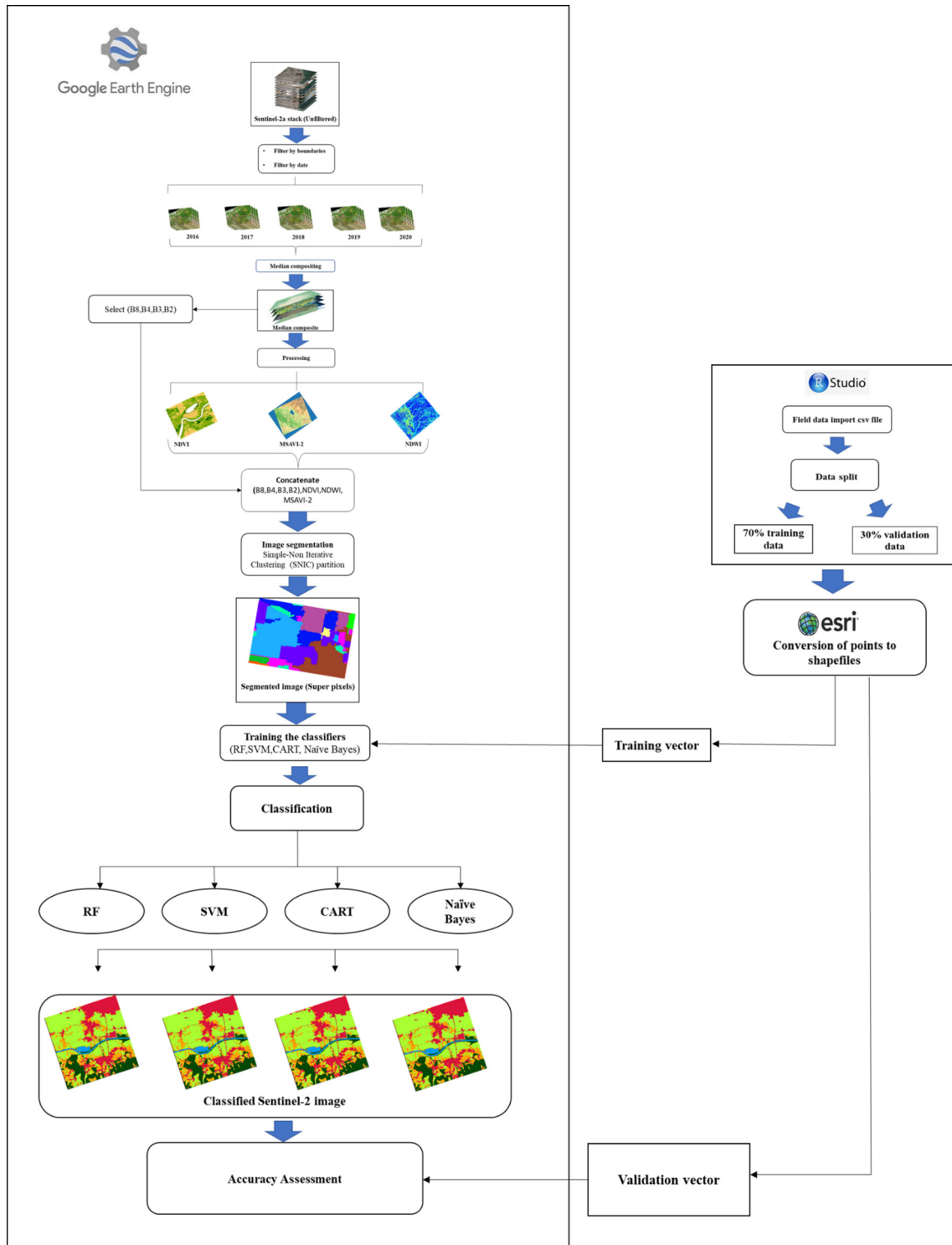

Fig. 2. Steps undertaken to characterise and map the two wetlands using GEE.

filtering process. The acquired image stack was then normalised for illumination effects (i.e., shades) and minimisation of clouds, using median compositing. The median composite works by reducing a stack of images through the calculation of median of all values at each pixel across the stack of all matching bands thus minimising the effects of shades and clouds (Mahdianpari et al., 2019). The median composite in this study was executed using the code Median () on the GEE. This was then used to calculate the Normalised Difference Vegetation Index (NDVI), Normalised Difference Water Index (NDWI), and Modified Soil Adjusted Vegetation Index 2 (MSAVI-2), using the equations given in Table 1. The NDVI is one of the most widely used vegetation index in wetlands studies due to the sensitivity to photosynthetically active biomass and can discriminate between vegetation and non-vegetation as well as wetland from non-wetland features (Liu and Huete, 1995). The NDWI was selected due to sensitivity to open water enabling the discrimination of water from land surfaces (McFeeters, 1996). MSAVI-2 was chosen to improve the limitations of the NDVI. In addition to the extracted indices, the Near infrared (NIR), Red, Green and Blue bands were selected and concatenated to the NDVI, NDWI and MSAVI-2 outputs to produce an image with only the bands for wetlands classification. The NIR band was chosen because of its usefulness in distinguishing water from land surface as well as its ability to discern biomass content of vegetation and its health because water absorb strong NIR light while vegetation strongly reflects NIR light. The Red band was chosen because of its ability to delineate wetland classes because of its ability to detect chlorophyll absorption in vegetation. Blue band has the ability to differentiate between soils and vegetation. The produced composite was then subjected to Object Based Image Analysis (OBIA). OBIA was selected because of the superiority against pixel-based classification as shown in various wetlands mapping studies such as Berhane et al. (2018), Kamal and Phinn (2011) and Kaplan and Avdan (2017). Moreover, the approach not only relies on spectral characteristics of each pixel but also considers other pixel characteristics, such as size, shape and contextual information thus improving spectral separability within classes of the heterogeneous wetlands (Halabisky, 2011). The first step in OBIA is image segmentation. The process involves partitioning of the image into multiple discreet and non-overlapping segments based on a specific criterion (Dlamini et al., 2021). In this process, individual pixels are merged to produce larger objects. This increases the discrimination of spectrally similar objects using texture, shape and contextual features and prevents the "salt and pepper" noise in the final classification map (Dlamini et al., 2021; Mahdianpari et al., 2020). In this study, a Simple Non-Iterative Clustering (SNIC) algorithm was used to segment the composite. The SNIC algorithm was chosen because of its simplicity, memory efficiency, processing speed as well as the ability to incorporate connectivity between pixels after the algorithm has been initiated (Achanta and Süsstrunk, 2017). The SNIC algorithm starts the process of image segmentation by initialising the centroids pixels on a regular grid image, then the dependency of each pixel relative to the centroids is established using the distance in five-dimensional space of colour and spatial coordinates. In particular, the distance integrates normalised spatial and colour distances to produce uniform super pixels (Achanta and Süsstrunk, 2017). The candidate pixel is selected based on the

shortest distance from the centroid (Achanta and Süsstrunk, 2017). The SNIC algorithm was executed using the code ee.Algorithms.Image. Segmantation.SNIC () on GEE and the output was an image with super pixels, calculated textures, areas, sizes and perimeters for all the super pixels.

3.3. Adopted wetland classification scheme

Satellite image classification was executed, using the Random Forest (RF), Support Vector Machine (SVM), Classification and Regression Tree (CART) and Naïve Bayes (NB) algorithms. The RF is an ensemble classifier, which consists of a combination of tree classifiers, and each classifier is generated using the random factor sampled independently from the input vector data. Each tree cast a unit vote for a popular class to classify an input vector (Ao et al., 2019; Pal, 2005). An advantage of RF algorithm is the ability to handle large differentiations within landcover classes, and noise data can be neutralised (Slagter et al., 2020). Moreover, the algorithm does not require the understanding of the data distribution unlike the parametric classification algorithms such as maximum likelihood, where data distribution needs to be known. The SVM applies a sophisticated kernel function to classify data sets with complex decision surface. One of the strengths of SVM is that the uncertainty in model structure is decreased and similar to RF the algorithm also does not rely on the data distribution (Oommen et al., 2008). CART is a tree-based classification algorithm that measures the dependence relation of one variable to other variables (Simioni et al., 2020). An advantage of CART is the ability to naturally model non-linear boundaries because of its hierarchical structure. NB forms part of simple probabilistic classifiers based on applying Bayes theorem with strong independence assumption between features (Shelestov et al., 2017; Simioni et al., 2020). An advantage of NB algorithm includes the ability to solve multi-class prediction problems, time saving as well as less training data requirements. The four algorithms were chosen because of the latter advantages in addition to their acceptable performance demonstrated in several land cover studies such as Dlamini et al. (2021); Rana and Venkata Suryanarayana (2020); Rodriguez-Galiano et al. (2012); Simioni et al. (2020); Slagter et al. (2020). Moreover, studies such as Hayri Kesikoglu et al. (2019) and Tian et al. (2016) reported that application of the latter algorithms on mapping semi-arid wetlands is limited, hence these were selected. Prior to classification, the algorithms were trained using 70% of the field data. The data were randomly split in R-studio to produce a 70% training set, and 30% validation set. The code used to split data in R-studio is "wasdt = sort(sample(nrow (data), nrow(data)*.7))". After splitting, the data were converted to GIS files in Esri ArcGIS 10.2, and then imported to GEE for modeling training and validating. The training of the classifiers was executed using the code "ee.Classifier.train ()". Classification using the latter algorithms was then implemented on the segmented image using the code "Image.classify()" in GEE.

3.4. Accuracy assessment

In evaluating the performance of classification algorithms, three evaluation indices were used. These are overall accuracy (OA),

Table 1
Features extracted from the optical data.

Data	Data extracted	Formula	Band width (nm)	Reference
Sentinel-2	B8 - Near-infrared (NIR)		842	
	B4 - Red		665	
	B3 – Green		560	
	B2 – Blue		490	
	Normalised Difference Vegetation Index (NDVI)	$\frac{NIR-Red}{NIR+Red}$	–	(Liu and Huete, 1995)
	Normalised Difference Water Index (NDWI)	$\frac{NIR-Green}{NIR+Green}$	–	(McFeeters, 1996)
	Modified Soil Adjusted Vegetation index (MSAVI-2)	$\frac{2\times NIR+1-\sqrt{(2\times NIR+1)^2-8\times(NIR-Red)}}{2}$	–	(Qi et al., 1994)

producer's accuracy and user's accuracy. In addition, line graphs as well as Jeffries-Matusita (JM) distances were used to establish the separability of different wetland classes using the selected spectral bands. JM is a parametric criterion that ranges between 0 and 2. This criterion uses distances (Eqs. (1) & (2)) between the class means and the distribution of values from the means to assess the separability of one class from the other (Dabboor et al., 2014; Wang et al., 2018). Distances approaching 2 indicate a greater average distance between two classes and therefore separable using the data type. The OA was used to measure the efficiency of used algorithms and was quantified as the ratio of total correctly labelled samples and the total number of testing samples. The producer's accuracy was used to measure the probability that the reference sample is correctly classified on the map. The user's accuracy was used as an indicator of the probability that a classified pixel in the wetland cover classification map accurately represents that category on the ground. The accuracy assessments with the latter indices were computed executed in GEE. The JM distance presented in Dabboor et al. (2014) is given as:

$$JM = 2\left(1-e^{-B}\right) \tag{1}$$

where B is the Bhattacharyya distance and quantified as

$$B = \frac{1}{8}\left(\mu_i-\mu_j\right)^T\left(\frac{\Sigma_i+\Sigma_j}{2}\right)^{-1}\left(\mu_i-\mu_j\right) + \frac{1}{2}\ln\left(\frac{|(\Sigma_i+\Sigma_j)/2|}{\sqrt{|\Sigma_i||\Sigma_i|}}\right) \tag{2}$$

where μ_i and Σ_i are the mean and covariance matrix of class i and μ_j and Σ_j are the mean and covariance of class j. In evaluating the classification accuracy of the output image using the latter indices, the codes "Image. accuracy()" for OA, "Image.producersAccuracy()" for producer's accuracy and "Image.consumersAccuracy()" for user's accuracy were implemented on the GEE. During implementation of the latter codes, firstly,

the validation vector data were imported to the GEE and used to sample out the corresponding regions on the classified image using the code "Image.sampleRegions()". The sampled regions were then used in the latter codes as input image to test the accuracy of the classification outputs. The line plots and JM distances were implemented using a series of interconnected codes presented in the supplementary material.

4. Results

4.1. Class separability

Scatter plots (Fig. 3) showing spectral reflectance values per class of the studied wetlands indicate that most wetland classes are not distinguishable using Band 2, Band 3, and Band 4 for both wetlands except long grass in the Nylsvley flood plain, which was discernible from the rest of the classes using B4 and B8. The results also indicate that the Water class in the Lindani valley bottom has high spectral reflectance in the NIR region although the anticipation was low reflectance in this spectral region.

The JM distances obtained from the multi-year median composite (Tables 2 and 3), indicate that wetland features were hardly distinguishable from single optical bands for both wetlands. The least distinguishable classes were Bare surface and Water from the Lindani valley bottom as well as Bare surface and Short grass from the Nylsvley floodplain. The JM distances for all the least distinguishable classes were not exceeding 1.4 for both wetlands. The results also show that synergic use of all optical features significantly increased the separability between classes with JM distances exceeding 1.8 for both wetland classes.

4.2. Classification results and accuracies

Four GEE algorithms were applied to a median composite of Sentinel-2 images to produce custom maps for two seasonal flooded
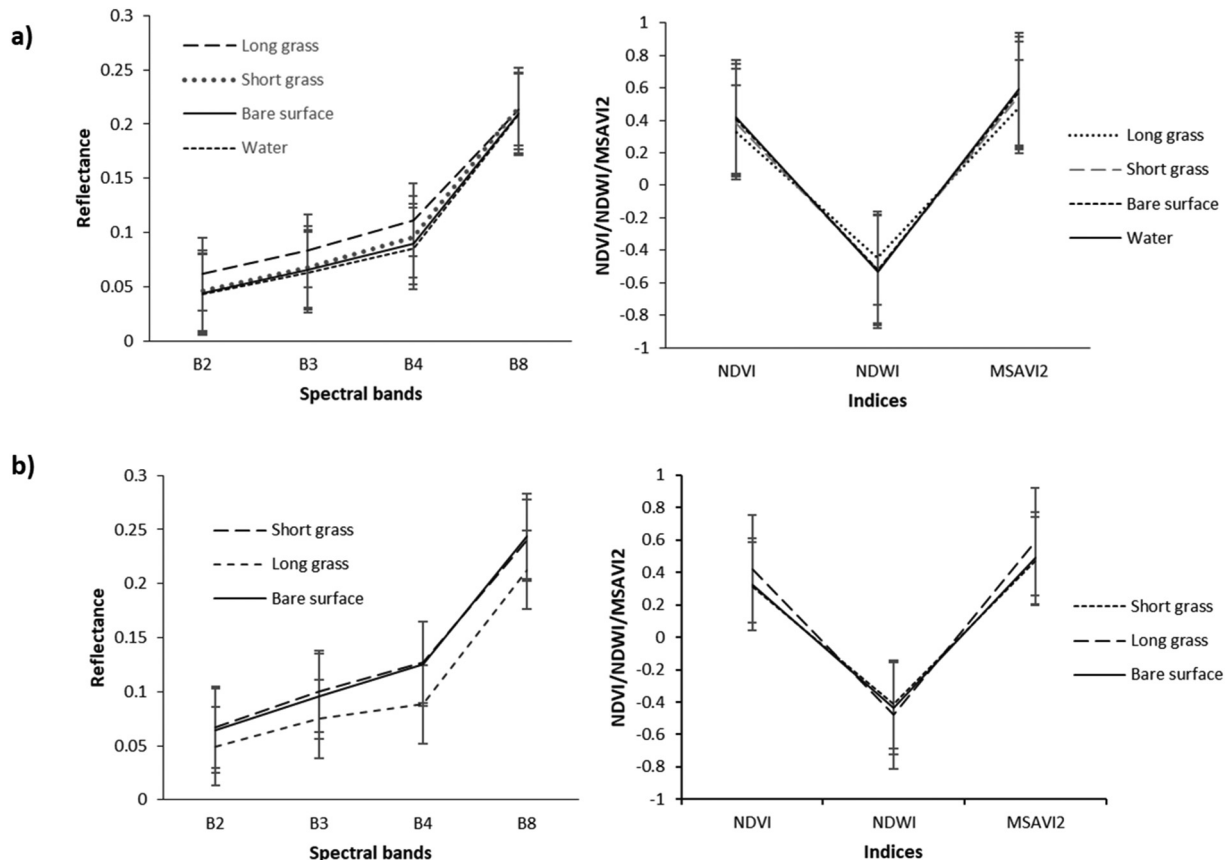

Fig. 3. Wetland cover class spectral reflectance values for a) Lindani valley bottom and b) Nylsvley floodplain, using pixel values extracted from the training data.

Table 2
JM distances between wetland cover classes in the Lindani valley bottom.

Optical features	D1[a]	D2[b]	D3[c]	D4[d]	D5[e]	D6[f]
NIR	0.0016	0.0131	0.1036	0.0135	1.272	0.1398
Red	0.3146	0.4311	0.5635	0.0502	0.1576	0.0314
Green	0.4331	0.6508	0.8978	0.0600	0.2714	0.0966
Blue	0.4675	0.6381	0.8861	0.0418	0.2193	0.0858
NDVI	0.2728	0.3044	0.6300	0.0385	0.1823	0.1127
NDWI	0.3478	0.4028	0.4346	0.0036	0.0168	0.0089
MSAVI2	0.3124	0.3509	0.6849	0.0041	0.1948	0.1187
ALL	2	2	2	2	2	2

[a] D1: Long grass & Short grass.
[b] D2: Long grass & Bare surface.
[c] D3: Long grass & Water.
[d] D4: Short grass & Water.
[e] D5: Short grass and Water.
[f] D6: Bare surface and Water.

Fig. 4. Overall Accuracy comparison between the algorithms used.

wetlands of variable sizes in the LTRB. Figs. 7 and 8 show the custom maps for the studied wetlands. Overall Accuracies based on the algorithms used ranged between 20% and 80% for both wetlands, with Random Forest (RF) having high OA for both Lindani valley bottom and Nylsvley floodplain (68.80% and 80.55%) and Naïve Bayes (NB) having the low OA values for both wetlands (29.50% and 25.00%) (Fig. 4). The other algorithms had reasonable accuracy with the Support Vector Machine (SVM) attaining 66.60% for Lindani and 62.29% for Nylsvley. The Classification and Regression Tree (CART) achieved an OA of 62.30% for Lindani and 75.00% for Nylsvley, thus proving the superiority of RF amongst other algorithms used in this study.

Figs. 7 and 8 show the distribution of wetland cover classes at 10 m spatial resolution. The maps illustrate fine separation between the wetland classes for all the algorithms. However, for the Nylsvley floodplain, the water class could not be detected due to the unavailability of training data representing this class. The areas of the various land cover types in Fig. 5 show that based on all the algorithms except NB, the most dominating class in the Lindani valley bottom is Short grass consisting of *Cynodon dyctolon* and *Oryza longistaminata*. In contrast, the NB identified water as being the most dominant class. The area of the short grass ranged between 5 ha and 25 ha with the NB model identifying the smallest area for this cover type. The producer's accuracy and user's accuracy for the dominating short grass ranged between 20% and 91%, with NB model having the lowest producer's accuracy (Fig. 6), and the user's accuracy was from 60% to 80% with SVM having the lowest accuracy. The least dominating classes in the Lindani valley bottom wetland are water and bare surface with areas ranging of 0.3–5.0 ha for bare surface and 0.2–10.0 ha for water. The producer's accuracies for these two classes ranged between 0% and 75% for water and between 0% and 30% for bare surface. The SVM algorithm achieved 0% producer's accuracy for both the classes. The user's accuracy for the two classes was from 0% to 75% for bare surface and 0% to 50% for water. The SVM algorithm had a 0% user's accuracy for both classes (Fig. 6). The dominating landcover class in the Nylsvley floodplain is bare surface with an estimated area ranging from 362 ha to 495 ha.

The CART algorithm estimated the lowest area. The least dominating class is long grass comprising mainly common reeds species such as *Phragmites australis*. The area for the least dominating wetland cover class ranged between 130 ha and 352 ha. The highest area was estimated by CART, and the lowest by NB. The producer's accuracy for the dominating class ranged between 62% and 88% with the highest being attained by the NB and the lowest by the SVM model. The producer's accuracy for the least dominating class ranged between 33% and 66.6% with the highest attained by NB model and lowest by CART and RF models. The user's accuracy for the most dominating class ranged between 22% and 71% with highest recorded by SVM and CART and the lowest by the NB model. User's accuracy for the least dominating ranged between 20% and 66.6% with highest recorded by RF and lowest by CART.

5. Discussion

Accurate detection and monitoring of small seasonal and heterogeneous wetlands in the semi-arid regions is important for understanding the ecohydrological dynamics of these systems, as most of these wetlands particularly in the sub-Saharan Africa offer socio-economic benefits to the surrounding communities (Gardner et al., 2009; Kabii and Kabii, 2005; Thamaga et al., 2021). Advancements in data analytic tools provide unique opportunities to improve the detection and monitoring of semi-arid wetlands of variable sizes, which were not feasible, using the traditional remote sensing techniques. The introduction of cloud computing platforms such as Google Earth engine (GEE), offers advantages such as advanced machine learning algorithms and parallel processing, memory efficiency and fast image processing power. The study sought to assess the capabilities of GEE cloud-computing platform in characterizing and mapping semi-arid seasonally flooded wetlands at site specific scale, as well as suggesting a suitable GEE machine learning algorithm for characterizing and mapping such systems.

In general, the results demonstrate the capabilities of Google Earth engine cloud computing platform in characterizing and mapping the semi-arid wetland systems of variable sizes with acceptable overall accuracies. In addition, RF, CART and SVM algorithms proved to be superior to the NB model with low OA values for both studied wetlands. Although higher OA were obtained using the latter algorithms, low producer's and user's accuracies occurred in the Lindani valley bottom for Bare and Water classes, especially using SVM model. The contributing factors to the low producer's and user's accuracies for the two classes were few training and validation sample points representing these classes due to less than a pixel spatial coverage of each class within the wetland boundary. Fewer training and validation points tend to reduce the

Table 3
JM distances between wetland cover classes in the Nylsvley floodplain.

Optical features	D1[a]	D2[b]	D3[c]
NIR	0.2586	0.3839	0.0342
Red	0.6208	0.5998	0.0016
Green	0.6913	0.5289	0.0226
Blue	0.7211	0.5828	0.0251
NDVI	0.5663	0.5534	0.0358
NDWI	0.6675	0.3876	0.1351
MSAVI2	0.5986	0.0038	0.0524
ALL	2	2	1.990

[a] D1: Short grass & Long grass.
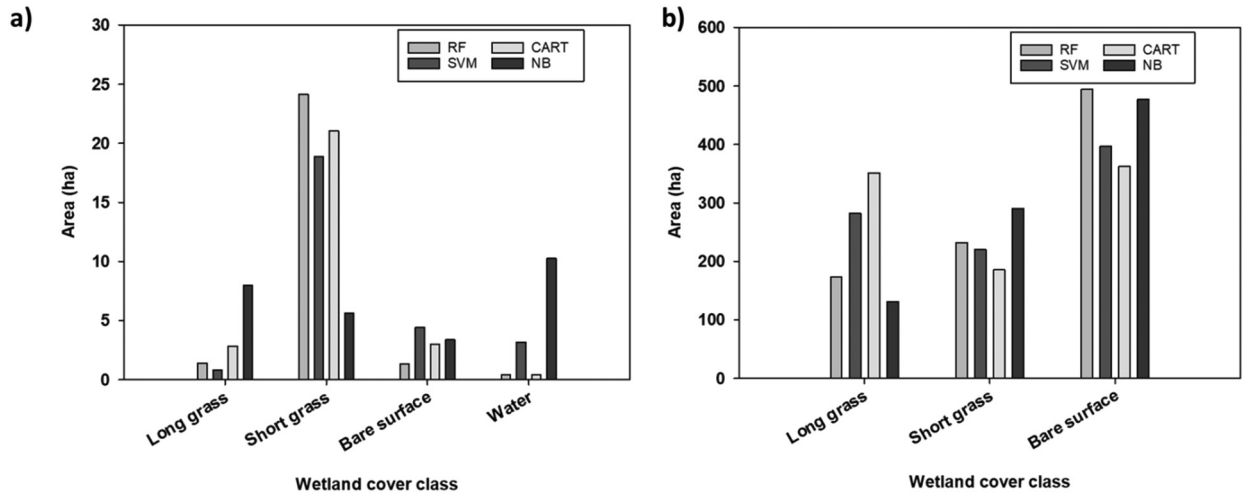[b] D2: Long grass & Bare.
[c] D3: Bare surface & Short grass.

Fig. 5. Wetland cover class areas for a) Lindani valley bottom and b) Nylsvley floodplain.

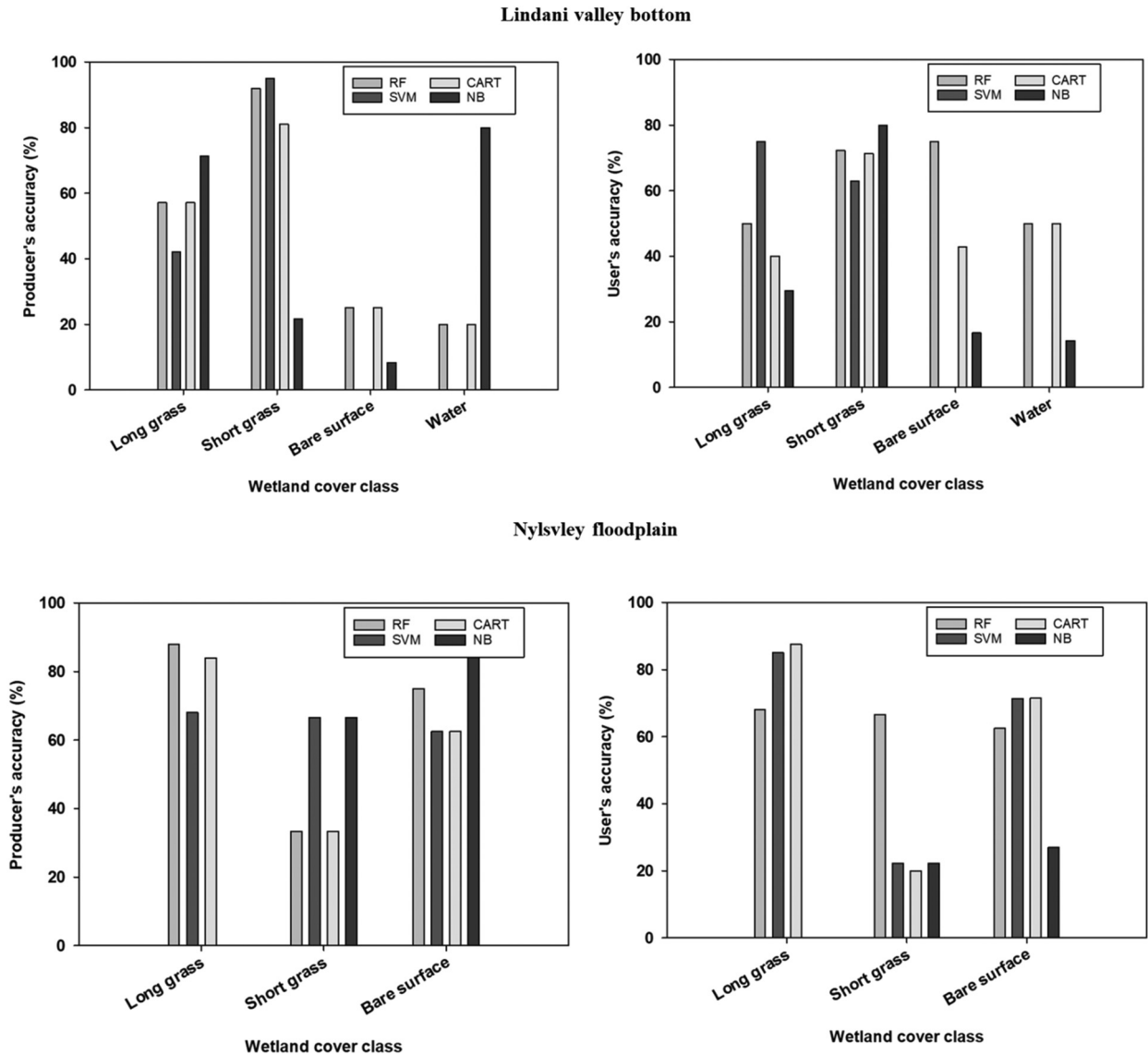**Lindani valley bottom**

Nylsvley floodplain

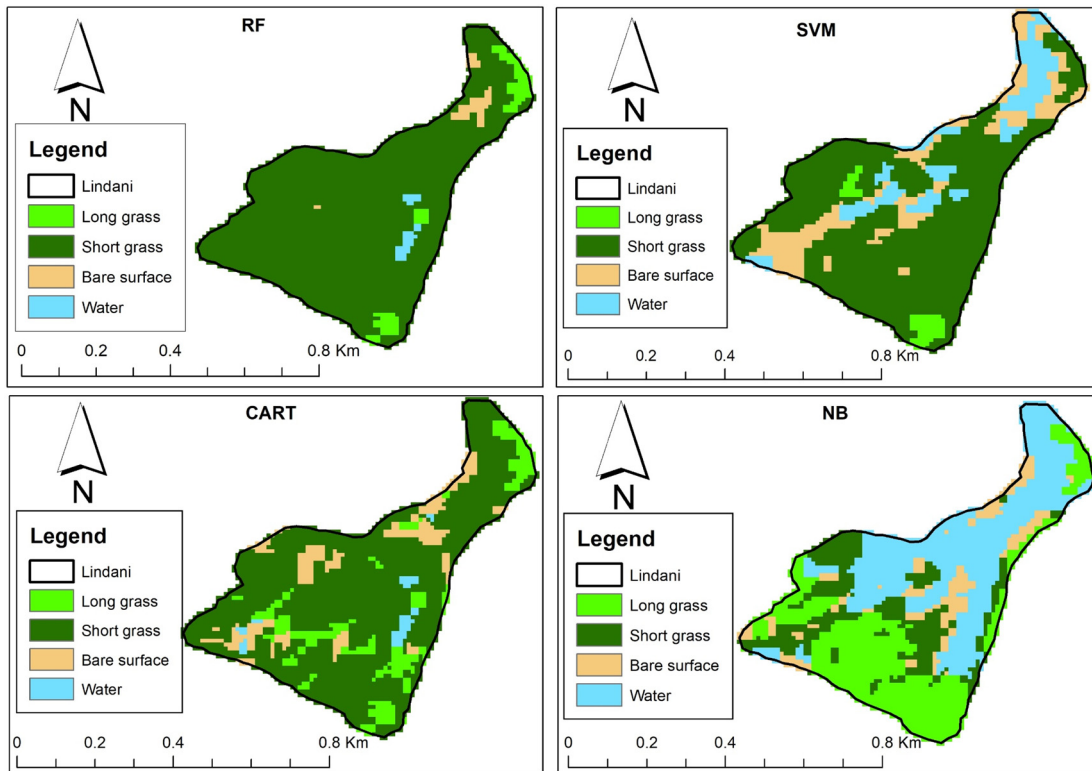**Fig. 6.** Producer's and user's accuracy for the two wetlands classes.

Fig. 7. Lindani valley bottom Sentinel 2 derived wetland cover classes based on the four used algorithms.
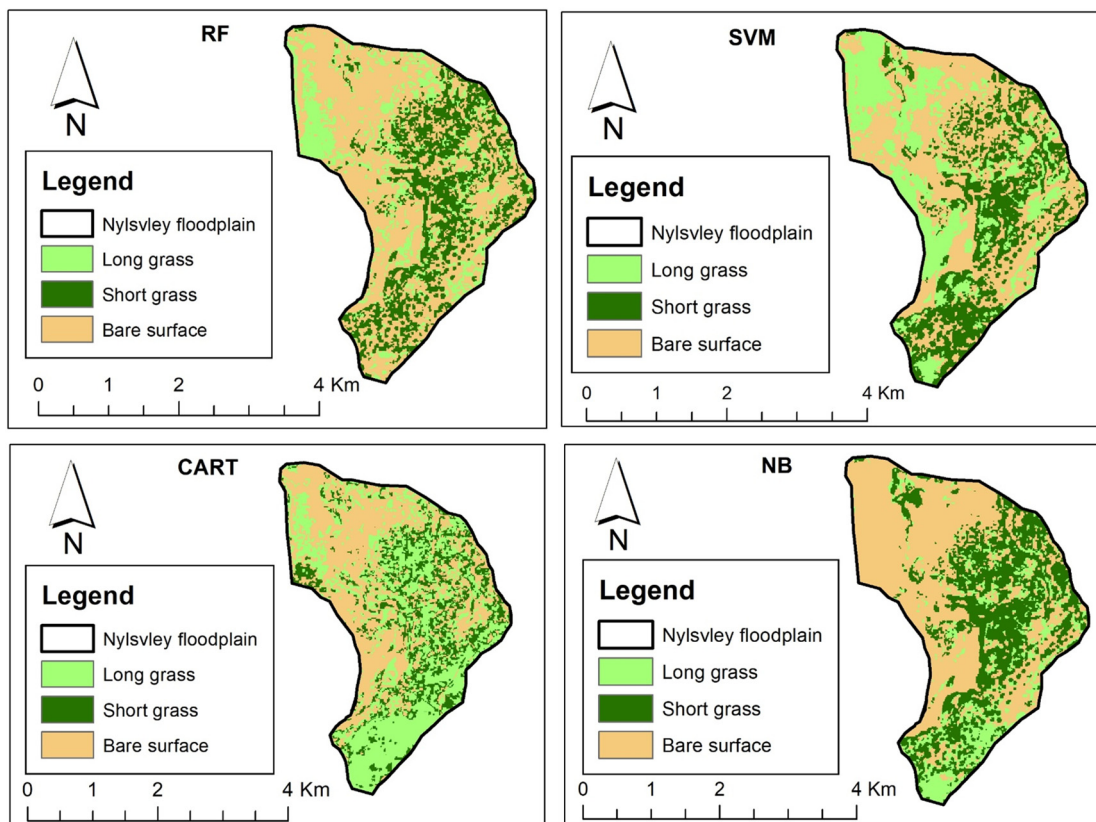

Fig. 8. Nylsvley Floodplain Sentinel 2 derived wetland cover classes based on four algorithms used.

level of accuracy during classification (Corcoran et al., 2015; Mahdianpari et al., 2020; Zhen et al., 2013). In addition to few training and validation data points, the multi-year images used during the computation of median composite did not consider seasonality and yearly differences, and that may have reduced the producer's and user's accuracies. The study by Noi Phan et al. (2020) analysed the impact of different composition methods as well as input images on the classification accuracy of different landcover classes using GEE. The results showed that temporal aggregation considered during median compositing produced high accuracy values for the classification outputs. This demonstrates the significance of temporal aggregations during the median compositing stage. Although the results underscore the relevance of the GEE cloud computing platform in characterizing and mapping small seasonal flooded wetlands in the semi-arid regions, there are some limitations associated with the use of this platform. These include computational restrictions where large trainings required by complex machine learning algorithms cannot be performed due to space limitations, unavailability of complex and accurate image segmentation algorithms as well as restricted image processing tools. Moreover, the algorithms used have limitations such as, slow training and biasness when dealing with categorical data in the case of RF, under performance when dealing large data in case of SVM, more time required to train the model in the case of CART and dependencies amongst classes cannot be modelled when using NB.

Class spectral separability results show that the use of single optical bands and indices in differentiating between the wetland classes for all bands, not feasible in this case, although spectral bands such as NIR and Red are known to be useful in wetlands delineation, vegetation, soil and geology studies (Amani et al., 2018). Water was expected to be easily discernible from other classes as it is known to have strong NIR adsorption and Low NIR reflectance making it easy to discriminate it from other classes such as vegetation and soils which reflect more light at NIR region. A study by Amani et al. (2018) reported great separability of wetland cover classes using the NIR band particularly shallow waters of the Newfoundland in semi-arid Canada. Red Band is known to be useful in detecting chlorophyll absorption in vegetation as well as the composite of soils, where soils with rich iron oxide will have stronger reflectance and healthy vegetation will absorb red light, making it easy to separate these classes from water. The results by Amani et al. (2019) show that the shallow water of the Newfoundland wetlands in Canada were discernible from the other classes such as soils and vegetation using the Red Band, however it was highlighted that in some instances it may not be easy to discriminate these classes due to similarities in spectral reflectance.

The synergic use of all spectral features significantly increased the separability of different classes for both wetlands with JM distances above 1.9. However, in the NIR region the logical expectation was that vegetation and water will have strong reflectance and adsorption in the NIR region, but in the case of Lindani valley bottom, water had stronger reflectance in this spectral region. This could be due to the submerged and floating wetland vegetation that interfere with the water signals thus causing stronger reflectance of water at NIR region (De Vries et al., 2017). In addition, materials at the bottom of the shallow waters are known to affect absorption and reflectance of light by shallow waters (Vincíková et al., 2015). This could also be the case for this wetland with shallow water. Jones (2015), reported increased errors in mapping the spatial extent of water in areas within the greater Everglades where vegetation is floating. This showed the problem of discriminating between water and vegetation in such wetlands. In the study presented in this paper, both wetlands had short and long grass classes with higher reflectance values in the visible red-light region indicative of water stressed vegetation. Water stressed vegetation is known to have stronger reflectance signals in visible red-light region (Adam et al., 2010; Macarthur, 1975). The study by Caturegli et al. (2020) assessed the effects of water stress on spectral reflectance of Bermudagrass (*Cynodon dyctolon*) under controlled laboratory

conditions. The results showed an increase in red light reflectance with increasing water stress, thus proving that water stressed vegetation has a stronger reflectance in the visible red-light region. The indices were found to be the least useful in separating the class for both wetlands, partly because seasonality and yearly differences were not considered during median compositing of the selected images. Maximum NDVI values tend to correspond to the growing season in most cases. A study by Wang et al. (2020) examined the response of the maximum NDVI values to precipitation occurring during the period of active growth from 2000 to 2013 in the Alpine grassland site of the Tibetan Plateau. The results showed a positive linear relationship between precipitation and the maximum NDVI thus proving that NDVI is most useful during the peak growing season.

The findings of this study prove that the GEE platform and advanced machine learning algorithm have the potential to improve the detection and monitoring of small seasonally flooded wetlands in semi-arid regions using Sentinel-2 multi-year composite image. This has been previously a daunting task, using the conventional mapping methodologies and optical data. In addition, the results demonstrate that the most detectable wetland features were mostly wetland vegetation communities, although there were some challenges relating to accuracy particularly for the Lindani valley bottom system. The study provides baseline information and new insights about better enhancing small seasonal flooded wetlands from optical data at reasonable accuracy and moderately high-resolution, thus underscoring the significance of freely available optical data in monitoring semi-arid seasonal flooded systems. This is important for semi-arid regions with limited data access particularly sub-Saharan Africa where less attention is given to these systems due to limited information regarding their status although serving as important source of water for most communities. The findings also contribute towards the ongoing global wetland monitoring programmes such as Wetland Monitoring and Assessment Services for Transboundary Basins in Southern Africa (WeMAST) funded by European Union- Africa Global Monitoring for Environmental Security (EU Africa GMES). This programme aims at developing an integrated platform for wetlands assessment and monitoring that will support sustainable management in transboundary basins. Furthermore, the study contributes to the sustainable development goal 6.6, seeking to halt degradation and destruction of ecosystems including wetlands and assist in recovery of the already degraded systems.

6. Conclusion and recommendations

The current study was aimed at characterizing and mapping two seasonal flooded wetlands in the Limpopo Transboundary River Basin, with the objective of assessing the usefulness of GEE cloud computing platform in producing maps of the studied wetlands as well as suggesting possible GEE algorithms for detecting and mapping such systems. The main findings indicate the capabilities of GEE in mapping seasonal semi-arid wetlands system of variable size with reasonable overall accuracies, and RF CART and SVM algorithms being superior to the NB model. Although reasonable overall accuracies were attained, there were poor producer's and user's accuracies for some classes such as Water and Bare surface especially for the Lindani valley bottom wetland. This can be attributed to less than a pixel spatial coverage of these classes within wetlands perimeter, thus resulting in difficulties in their detection to the highest precision using Sentinel-2 composite data. In addition, the seasonality and yearly difference were not considered which could have significantly affected the results because some features such as water tend to correspond to seasonality changes, especially for semi-arid season. It is therefore recommended that temporal variability be considered in-order to capture the peak growing season of the systems and thus better enhancing the wetland features. Spectral confusions were also observed between water and some wetland vegetation, which resulted in the higher reflectance of water in the NIR region. In avoiding such, the study recommends the integration of

Synthetic Aperture Radar (SAR) data to the optical data since SAR data can penetrate through forested vegetation thus minimising the effect of floating vegetation in the detection of water class. Moreover, the testing of other machine learning algorithms such as Artificial Neural Network (ANN) as well as the inclusion of Short-wave infrared and thermal bands are recommended.

CRediT authorship contribution statement

Conceptualization, T.D. and D.M.; writing-original draft preparation, S.G.; writing, reviewing and editing, T.D., and D.M.; funding acquisition, T.D and D.M. All authors have read and agreed to the published version of the manuscript.

Declaration of competing interest

The authors declare that they have no known competing financial interests or personal relationships that could have appeared to influence the work reported in this paper.

Appendix A. Supplementary data

Supplementary data to this article can be found online at https://doi.org/10.1016/j.scitotenv.2021.150139.

References

Achanta, R., Süsstrunk, S., 2017. Superpixels and polygons using simple non-iterative clustering. Proceedings - 30th IEEE Conference on Computer Vision and Pattern Recognition, CVPR 2017, pp. 4895–4904 https://doi.org/10.1109/CVPR.2017.520.

Adam, E., Mutanga, O., Rugege, D., 2010. Multispectral and hyperspectral remote sensing for identification and mapping of wetland vegetation: a review. Wetl. Ecol. Manag. 18, 281–296. https://doi.org/10.1007/s11273-009-9169-z.

Amani, M., Salehi, B., Mahdavi, S., Brisco, B., 2018. Spectral analysis of wetlands using multi-source optical satellite imagery. ISPRS J. Photogramm. Remote Sens. 144, 119–136. https://doi.org/10.1016/j.isprsjprs.2018.07.005.

Amani, M., Brisco, B., Afshar, M., Mirmazloumi, S.M., Mahdavi, S., Mirzadeh, S.M.J., Huang, W., Granger, J., 2019. A generalized supervised classification scheme to produce provincial wetland inventory maps: an application of Google earth engine for big geo data processing. Big Earth Data 3, 378–394. https://doi.org/10.1080/20964471.2019.1690404.

Amani, M., Ghorbanian, A., Ahmadi, S.A., Kakooei, M., Moghimi, A., Mirmazloumi, S.M., Moghaddam, S.H.A., Mahdavi, S., Ghahremanloo, M., Parsian, S., Wu, Q., Brisco, B., 2020. Google earth engine cloud computing platform for remote sensing big data applications: a comprehensive review. IEEE J Sel. Top. Appl. Earth Obs. Remote Sens. 13, 5326–5350. https://doi.org/10.1109/JSTARS.2020.3021052.

Ao, Y., Li, H., Zhu, L., Ali, S., Yang, Z., 2019. The linear random forest algorithm and its advantages in machine learning assisted logging regression modeling. J. Pet. Sci. Eng. 174, 776–789. https://doi.org/10.1016/j.petrol.2018.11.067.

Berhane, T.M., Lane, C.R., Wu, Q., Anenkhonov, O.A., Chepinoga, V.V., Autrey, B.C., Liu, H., 2018. Comparing pixel- and object-based approaches in effectively classifying wetland-dominated landscapes. Remote Sens. 10. https://doi.org/10.3390/rs10010046.

Botai, C.M., Botai, J.O., Zwane, N.N., Hayombe, P., Wamiti, E.K., Makgoale, T., Murambadoro, M.D., Adeola, A.M., Ncongwane, K.P., de Wit, J.P., Mengistu, M.G., Tazvinga, H., 2020. Hydroclimatic extremes in the Limpopo River Basin, South

Africa, under changing climate. Water (Switzerland) 12, 1–20. https://doi.org/10.3390/w12123299.

Caturegli, L., Matteoli, S., Gaetani, M., Grossi, N., Magni, S., Minelli, A., Corsini, G., Remorini, D., Volterrani, M., 2020. Effects of water stress on spectral reflectance of bermudagrass. Sci. Rep. 1–12. https://doi.org/10.1038/s41598-020-72006-6.

Chen, M., Liu, J., 2015. Historical trends of wetland areas in the agriculture and pasture interlaced zone: a case study of the Huangqihai Lake Basin in northern China. Ecol. Model. 318, 168–176. https://doi.org/10.1016/j.ecolmodel.2014.12.012.

Corcoran, J., Knight, J., Pelletier, K., Rampi, L, Wang, Y., 2015. The effects of point or polygon based training data on randomForest classification accuracy of wetlands. Remote Sens. 7, 4002–4025. https://doi.org/10.3390/rs70404002.

Dabboor, M., Howell, S., Shokr, M., Yackel, J., 2014. The jeffries-matusita distance for the case of complex Wishart distribution as a separability criterion for fully polarimetric SAR data. Int. J. Remote Sens. 35, 6859–6873. https://doi.org/10.1080/01431161.2014.960614.

Day, J., Day, E., Ross-Gillespie, V., Ketley, A., 2010. The assessment of temporary wetlands during dry conditions, Wetland Health and Importance Research Programme. WRC Report no TT 439/09.

De Vries, B., Huang, C., Lang, M.W., Jones, J.W., Huang, W., Creed, I.F., Carroll, M.L., 2017. Automated quantification of surface water inundation in wetlands using optical satellite imagery. Remote Sens. 9. https://doi.org/10.3390/rs9080807.

Ding, C.S., Hsieh, C.T., Wu, Q., Pedram, M., 1998. Stratified random sampling for power estimation. Low-Power CMOS Design, pp. 501–507 https://doi.org/10.1109/9780470545058.sect13.

Dlamini, M., Adam, E., Chirima, G., Hamandawana, H., 2021. A remote sensing-based approach to investigate changes in land use and land cover in the lower uMfolozi floodplain system, South Africa. Trans. R. Soc. S. Afr., 1–13 https://doi.org/10.1080/0035919X.2020.1858365.

Dzurume, T., 2021. The Use of Remote Sensing Data for Assessing Water Quality in Wetlands Within the Limpopo River Basin. University of the Western Cape, Cape Town.

Gardner, R.C., Connolly, K.D., Bamba, A., Diana Connolly, K., Bamba, Abou, 2009. African Wetlands of International Importance: Assessment of African Wetlands of International Importance: Assessment of Benefits Associated with Designations under the Ramsar Benefits Associated with Designations under the Ramsar Convention Convention Afr. 21 Geo. Int'l. Envtl. L. Rev.257, pp. 1–39.

Gebresllassie, H., Gashaw, T., Mehari, A., 2014. Wetland degradation in Ethiopia: causes, consequences and remedies. J. Environ. Earth Sci. 4, 40–49.

Gorelick, N., Hancher, M., Dixon, M., Ilyushchenko, S., Thau, D., Moore, R., 2017. Google earth engine: planetary-scale geospatial analysis for everyone. Remote Sens. Environ. 202, 18–27. https://doi.org/10.1016/j.rse.2017.06.031.

Gxokwe, S., Dube, T., Mazvimavi, D., 2020. Multispectral remote sensing of wetlands in semi-arid and arid areas: a review on applications, challenges and possible future research directions. Remote Sens. 12, 1–19. https://doi.org/10.3390/rs12244190.

Halabisky, M., 2011. Object-based classification of semi-arid wetlands. J. Appl. Remote. Sens. 5, 053511. https://doi.org/10.1117/1.3563569.

Hayri Kesikoglu, M., Haluk Atasever, U., Dadaser-Celik, F., Ozkan, C, 2019. Performance of ANN, SVM and MLH techniques for land use/cover change detection at sultan marshes wetland, Turkey. Water Sci. Technol. 80, 466–477. https://doi.org/10.2166/wst.2019.290.

Jones, J.W., 2015. Efficient wetland surface water detection and monitoring via landsat: comparison with in situ data from the everglades depth estimation network. Remote Sens. 7, 12503–12538. https://doi.org/10.3390/rs70912503.

Kabii, T., Kabii, Tom, 2005. An Overview of African Wetlands Item Type Working Paper An Overview of African Wetlands. Available at: https://aquadocs.org/handle/1834/457. (Accessed 5 June 2021).

Kamal, M., Phinn, S., 2011. Hyperspectral data for mangrove species mapping: a comparison of pixel-based and object-based approach. Remote Sens. 3, 2222–2242. https://doi.org/10.3390/rs3102222.

Kaplan, G., Avdan, U., 2017. Mapping and monitoring wetlands using Sentinel-2 satellite imagery. ISPRS Ann. Photogramm. Remote Sens. Spat. Inf. Sci. 4, 271–277. https://doi.org/10.5194/isprs-annals-IV-4-W4-271-2017.

Kumar, L., Mutanga, O., 2018. Google earth engine applications since inception: usage, trends, and potential. Remote Sens. 10, 1–15. https://doi.org/10.3390/rs10101509.

Li, L., Vrieling, A., Skidmore, A., Wang, T., Muñoz, A.R., Turak, E., 2015. Evaluation of MODIS spectral indices for monitoring hydrological dynamics of a small, seasonally-flooded wetland in southern Spain. Wetlands 35, 851–864. https://doi.org/10.1007/s13157-015-0676-9.

Liu, H.Q., Huete, A., 1995. A feedback based modification of the NDVI to minimize canopy background and atmospheric noise. IEEE Trans. Geosci. Remote Sens. 33, 457. https://doi.org/10.1109/TGRS.1995.8746027.

Liu, D., Cao, C., Chen, W., Ni, X., Tian, R., Xing, X., 2017. Monitoring and predicting the degradation of a semi-arid wetland due to climate change and water abstraction in the Ordos Larus relictus National Nature Reserve, China. Geomatics Nat. Hazards Risk 8, 367–383. https://doi.org/10.1080/19475705.2016.1220024.

Macarthur, R., 1975. Geographic information systems and their use for environmental monitoring. In: Artiola, J., Pepper, I., Brusseau, M. (Eds.), Environmental Monitoring and Characterization. Elsevier Science & Technology Books, Amsterdam, pp. 86–100.

Mahdianpari, M., Salehi, B., Mohammadimanesh, F., Homayouni, S., Gill, E., 2019. The first wetland inventory map of newfoundland at a spatial resolution of 10 m using sentinel-1 and sentinel-2 data on the Google earth engine cloud computing platform. Remote Sens. 11. https://doi.org/10.3390/rs11010043.

Mahdianpari, M., Salehi, B., Mohammadimanesh, F., Brisco, B., Homayouni, S., Gill, E., DeLancey, E.R., Bourgeau-Chavez, L., 2020. Big data for a big country: the first generation of Canadian wetland inventory map at a spatial resolution of 10-m using Sentinel-1 and Sentinel-2 data on the Google earth engine cloud computing platform. Can. J. Remote. Sens. 46, 15–33. https://doi.org/10.1080/07038992.2019.1711366.

McFeeters, S.K., 1996. The use of the normalized difference water index (NDWI) in the delineation of open water features. Int. J. Remote Sens. 17, 1425–1432. https://doi.org/10.1080/01431169608948714.

Mosase, E., Ahiablame, L., Srinivasan, R., 2019. Spatial and temporal distribution of blue water in the Limpopo River basin, southern Africa: a case study. Ecohydrol. Hydrobiol. 19, 252–265. https://doi.org/10.1016/j.ecohyd.2018.12.002.

Noi Phan, T., Kuch, V., Lehnert, L.W., 2020. Land cover classification using Google earth engine and random forest classifier-the role of image composition. Remote Sens. 12. https://doi.org/10.3390/RS12152411.

Oommen, T., Misra, D., Twarakavi, N.K.C., Prakash, A., Sahoo, B., Bandopadhyay, S., 2008. An objective analysis of support vector machine based classification for remote sensing. Math. Geosci. 40, 409–424. https://doi.org/10.1007/s11004-008-9156-6.

Pal, M., 2005. Random forest classifier for remote sensing classification. Int. J. Remote Sens. 26, 217–222. https://doi.org/10.1080/01431160412331269698.

Qi, J., Chehbouni, A., Huete, A.R., Kerr, Y.H., Sorooshian, S., 1994. A modified soil adjusted vegetation index. Remote Sens. Environ. 48, 119–126. https://doi.org/10.1016/0034-4257(94)90134-1.

Rana, V.K., Venkata Suryanarayana, T.M., 2020. Performance evaluation of MLE, RF and SVM classification algorithms for watershed scale land use/land cover mapping using sentinel 2 bands. Remote Sens. Appl. Soc. Environ. 19, 100351. https://doi.org/10.1016/j.rsase.2020.100351.

Rodriguez-Galiano, V.F., Ghimire, B., Rogan, J., Chica-Olmo, M., Rigol-Sanchez, J.P., 2012. An assessment of the effectiveness of a random forest classifier for land-cover classification. ISPRS J. Photogramm. Remote Sens. 67, 93–104. https://doi.org/10.1016/j.isprsjprs.2011.11.002.

Ruiz, E., 2008. Management of Natura 2000 habitats * Mediterranean temporary ponds 3170. European Commission Report No. 2008 07/24.

Sawunyama, T., Senzanje, A., Mhizha, A., 2006. Estimation of small reservoir storage capacities in Limpopo River basin using geographical information systems (GIS) and remotely sensed surface areas: case of Mzingwane catchment. Phys. Chem. Earth 31, 935–943. https://doi.org/10.1016/j.pce.2006.08.008.

Shelestov, A., Lavreniuk, M., Kussul, N., Novikov, A., Skakun, S., 2017. Exploring Google earth engine platform for big data processing: classification of multi-temporal satellite imagery for crop mapping. Front. Earth Sci. 5, 1–10. https://doi.org/10.3389/feart.2017.00017.

Simioni, J.P.D., Guasselli, L.A., de Oliveira, G.G., Ruiz, L.F.C., de Oliveira, G., 2020. A comparison of data mining techniques and multi-sensor analysis for inland marshes delineation. Wetl. Ecol. Manag. 28, 577–594. https://doi.org/10.1007/s11273-020-09731-2.

Slagter, B., Tsendbazar, N.-E., Vollrath, A., Reiche, J., 2020. Mapping wetland characteristics using temporally dense Sentinel-1 and Sentinel-2 data: a case study in the St. Lucia wetlands, South Africa. Int. J. Appl. Earth Obs. Geoinf. 86, 102009. https://doi.org/10.1016/j.jag.2019.102009.

Tamiminia, H., Salehi, B., Mahdianpari, M., Quackenbush, L., Adeli, S., Brisco, B., 2020. Google earth engine for geo-big data applications: a meta-analysis and systematic review. ISPRS J. Photogramm. Remote Sens. 164, 152–170. https://doi.org/10.1016/j.isprsjprs.2020.04.001.

Thamaga, K.H., Dube, T., Shoko, C., 2021. Advances in satellite remote sensing of the wetland ecosystems in Sub-Saharan Africa. Geocarto Int., 1–22 https://doi.org/10.1080/10106049.2021.1926552.

Tian, S., Zhang, X., Tian, J., Sun, Q., 2016. Random forest classification of wetland landcovers from multi-sensor data in the arid region of Xinjiang, China. Remote Sens. 8, 1–14. https://doi.org/10.3390/rs8110954.

Vincikova, H., Hanuš, J., Pechar, L., 2015. Spectral reflectance is a reliable water-quality estimator for small, highly turbid wetlands. Wetl. Ecol. Manag. 23, 933–946. https://doi.org/10.1007/s11273-015-9431-5.

Wang, Y., Qi, Q., Liu, Y., 2018. Unsupervised segmentation evaluation using area-weighted variance and Jeffries-Matusita distance for remote sensing images. Remote Sens. 10. https://doi.org/10.3390/rs10081193.

Wang, J.W., Li, M., Zhang, G.Y., Zhang, H.R., Yu, C.Q., 2020. Growing season precipitation rather than growing season length predominates maximum normalized difference vegetation index in alpine grasslands on the Tibetan Plateau. Sustainability 12. https://doi.org/10.3390/su12030968.

Zhen, Z., Quackenbush, L.J., Stehman, S.V., Zhang, L., 2013. Impact of training and validation sample selection on classification accuracy and accuracy assessment when using reference polygons in object-based classification. Int. J. Remote Sens. 34, 6914–6930. https://doi.org/10.1080/01431161.2013.810822.